

Quasicontiguous frequency-fluctuation model for calculation of hydrogen and hydrogenlike Stark-broadened line shapes in plasmas

E. Stambulchik* and Y. Maron

Faculty of Physics, Weizmann Institute of Science, Rehovot 76100, Israel

(Received 26 November 2012; published 21 May 2013)

We present an analytical method for the calculation of shapes of Stark-broadened spectral lines in plasmas, applicable to hydrogen and hydrogenlike transitions (including Rydberg ones) with $\Delta n > 1$. The method is based on the recently suggested quasicontiguous approximation of the static Stark line shapes, while the dynamical effects are accounted for using the frequency-fluctuation-model approach. Comparisons with accurate computer simulations show excellent agreement.

DOI: [10.1103/PhysRevE.87.053108](https://doi.org/10.1103/PhysRevE.87.053108)

PACS number(s): 52.20.-j, 32.70.Jz, 32.30.-r, 32.60.+i

I. INTRODUCTION

Calculations of line shapes of hydrogen and hydrogenlike transitions (including Rydberg ones) are important for many topics of plasma physics and astrophysics. However, rigorous Stark broadening of the radiative transitions originating from high- n levels is rather complex, making the detailed calculations of their spectral structure very cumbersome. To overcome the difficulties, a simple analytical method for the calculation of line broadening was recently suggested [1], based on the quasicontiguous (QC) approximation of the static and quasistatic Stark line shapes. With further accounting for the dynamic properties of the plasma microfields, a simple expression for the full width at half maximum (FWHM) of the Stark line broadening in plasma was obtained.

In this study, the QC method is extended to analytical calculations of line *shapes* (not mere line *widths*) in plasmas. To this end, we employ a recent formulation [2] of the frequency fluctuation model (FFM). Although the new method is especially suitable for transitions with $\Delta n \gg 1$, it describes rather well even first members of the spectroscopic series with Δn as low as 2.

The paper is organized as follows. First, the QC-FFM method is developed assuming an ideal one-component plasma (OCP). Within this model, we briefly review the QC and FFM methods in Secs. II A and II B, respectively, followed by their combination in Sec. II C. In Sec. III we analyze the analytical expressions obtained, paying special attention to the collision-dominated regime. As expected, we do not recover the impact limit of the Stark broadening in this regime; however, a straightforward semi-empirical modification is found to correct this. Application of the method to nonideal multicomponent plasmas is described in Sec. IV, with a few examples of practical interest presented in Sec. V. Finally, the applicability of the method is discussed in Sec. VI and conclusions are drawn in Sec. VII.

II. IDEAL OCP

A. QC approximation

The detailed description of the QC approximation is given in Ref. [1]. For convenience, an abridged version is provided below.

For a dipole radiative transition between degenerate (hydrogenlike or Rydberg) levels with the principal quantum numbers n and n' , $n - n' \gg 1$, the static Stark shape caused by an electric field F can be accurately described by a rectangular shape (ω is relative to the zero-field line position ω_0),

$$I_{nn'}(\omega) = \begin{cases} \frac{I_{nn'}^{(0)}}{2\alpha_{nn'}F/\hbar} & \text{for } |\hbar\omega| \leq \alpha_{nn'}F, \\ 0 & \text{for } |\hbar\omega| > \alpha_{nn'}F, \end{cases} \quad (1)$$

where $I_{nn'}^{(0)}$ is the total line intensity, \hbar is the reduced Planck constant, and $\alpha_{nn'}$ is the linear-Stark-effect coefficient:

$$\alpha_{nn'} = \frac{3}{2}(n^2 - n'^2)\frac{ea_0}{Z}. \quad (2)$$

Here, e is the elementary charge, a_0 is the Bohr radius, and Z is the core charge of the radiator (in units of e). Evidently, the use of a single rectangular shape instead of a finite, but potentially large number of individual components, drastically reduces the complexity of the line-shape calculations and analysis.

We now proceed to evaluating the line shape in the quasistatic approximation. Convolution of Eq. (1) with a distribution of the field magnitudes $W(F)$ gives

$$I_{\text{qs}}(\omega) = I_{nn'}^{(0)} \int_{|\hbar\omega|/\alpha_{nn'}}^{\infty} \frac{W(F)dF}{2\alpha_{nn'}F/\hbar} \equiv I_{nn'}^{(0)} L_{\text{qs}}(\omega). \quad (3)$$

It is convenient to rewrite the area-normalized line shape $L_{\text{qs}}(\omega)$ using the reduced field strength $\beta = F/F_0$ and the reduced detuning $\bar{\omega} = \omega/\Delta_0$,

$$L_{\text{qs}}(\bar{\omega}) = \frac{1}{2} \int_{|\bar{\omega}|}^{\infty} \frac{\bar{W}(\beta)}{\beta} d\beta, \quad (4)$$

where

$$\Delta_0 = \frac{\alpha_{nn'}F_0}{\hbar}, \quad (5)$$

$$\bar{W}(\beta) = W(F)F_0, \quad (6)$$

*Evgeny.Stambulchik@weizmann.ac.il;
gate.weizmann.ac.il/

<http://plasma->

and F_0 is the Holtsmark normal field strength [3]:

$$F_0 = 2\pi \left(\frac{4}{15}\right)^{2/3} Z_p e N_p^{2/3}. \quad (7)$$

Here, Z_p and N_p are, respectively, the charge and the density of the perturber particles. In the limit of the ideal plasma (i.e., with omission of particle screening and other correlation effects), the distribution function $\bar{W}(\beta)$ becomes the Holtsmark function $H(\beta)$ [3]:

$$H(\beta) = \frac{2}{\pi} \beta \int_0^\infty x \sin(\beta x) \exp(-x^{3/2}) dx \quad (8)$$

(non-Holtsmark distributions are discussed in Sec. IV). In this case, the line shape according to Eq. (4) is merely

$$L_{qs}(\bar{\omega}) = S(\bar{\omega}), \quad (9)$$

where the S function is

$$S(\bar{\omega}) = \frac{1}{\pi} \int_0^\infty \cos(\bar{\omega} x) \exp(-x^{3/2}) dx. \quad (10)$$

Its Fourier transform¹ is

$$\mathcal{F}\{S(\bar{\omega})\}(\tau) = \exp(-|\tau|^{3/2}). \quad (11)$$

Defining half width at half maximum (HWHM) of $S(\bar{\omega})$ as $\bar{\omega}_{1/2}^0 \approx 1.44$, one can write the quasistatic full width at half maximum (FWHM) as

$$w_{qs} = 2\bar{\omega}_{1/2}^0 \Delta_0. \quad (12)$$

We note that the QC approximation cannot reproduce the central region of quasistatic line shapes, which is mainly determined by the single central component (Δn is odd) or the dip if it is absent (Δn is even). However, this region is very narrow ($\sim 1/n$ of the line width). Furthermore, even in this region the QC line shape is correct *on average*, therefore, adding a broadening of a small fraction of the line width is sufficient to eliminate the differences at large. This is demonstrated in Fig. 1, where relative differences between the quasistatic line shapes of Lyman $n = 9$ and $n = 10$ transitions and the QC one (10) are shown. It is seen that convolution with a Lorentzian as narrow as only one fifth of the line width results in QC line shapes that differ by only a few percent from the exact calculations. In reality, the source of such a broadening can be electrons or lighter ions in multicomponent plasmas (see Sec. IV below), or other broadening mechanisms, such as the Doppler or instrumental broadening.

Accounting for the influence of the microfield dynamics on the line width is done by introducing a ‘‘quasistaticity’’ factor f , defined as

$$f = \frac{R}{R + R_0}, \quad (13)$$

where

$$R = \frac{w_{qs}}{w_{dyn}} \quad (14)$$

¹Throughout the text, we assume the asymmetric notation with $(2\pi)^{-1}$ assigned to the inverse Fourier transform.

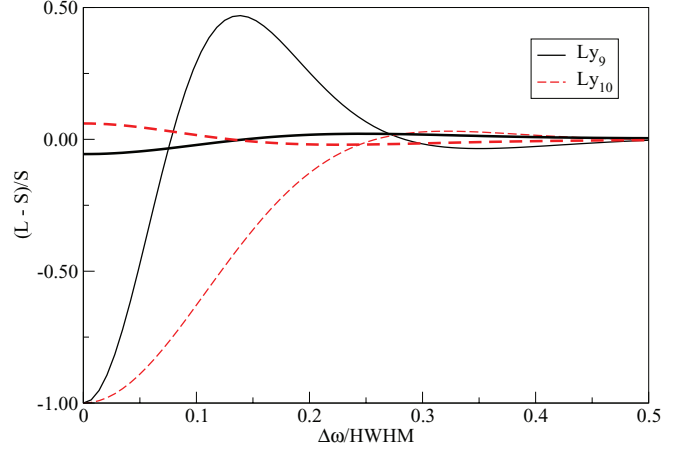


FIG. 1. (Color online) Thin lines: relative differences between the exact quasistatic Ly_9 and Ly_{10} shapes and the QC one (10) (the central component of the Ly_{10} line, which is a δ function in the nonquenching quasistatic approximation, is not shown); thick lines: same after convolution with a Lorentzian having $1/5$ width of the line FWHM.

is the ratio of the quasistatic width to the typical frequency of the microfield fluctuations w_{dyn} ,

$$w_{dyn} = \frac{\langle v \rangle}{\langle r \rangle} = \sqrt{\frac{kT}{m_p^*}} \left(\frac{4\pi N_p}{3} \right)^{1/3}. \quad (15)$$

Here, N_p , and m_p^* are, respectively, the density and the reduced mass of the perturbers. The dimensionless constant R_0 , determining transition from the quasistatic to dynamic regime, was inferred by comparisons with computer simulation results and found to be 0.5.

The full dynamic Stark width is then

$$w = f w_{qs}. \quad (16)$$

We note that the semi-empiric treatment of dynamic effects by Eqs. (13)–(16) has two important properties: (i) it gives the correct quasistatic width in the high-density/low-temperature limit and (ii) reproduces the expected T and N dependencies in the low-density/high-temperature impact limit [4],

$$w \propto N_p / \sqrt{T}. \quad (17)$$

B. FFM approximation

A recent formulation [2] of the original FFM approximation [5] is an attractive approach for very fast line-shape calculations. Departing from the quasistatic profile $L_{qs}(\omega)$, the dynamic line shape is given by

$$L(v; \omega) = \frac{1}{\pi} \operatorname{Re} \frac{\int \frac{L_{qs}(\omega') d\omega'}{v + i(\omega - \omega')}}{1 - v \int \frac{L_{qs}(\omega') d\omega'}{v + i(\omega - \omega')}}}, \quad (18)$$

where

$$v = C_0 w_{dyn} \quad (19)$$

and C_0 , similarly to R_0 in Eq. (13), is to be determined empirically by comparisons with computer simulation results [6].

The important features of Eq. (18) are (i) it preserves normalization, $\int L(\omega)d\omega = 1$; (ii) it recovers the quasistatic limit, i.e., at $\nu \rightarrow 0$, $L(\omega) \rightarrow L_{qs}(\omega)$; and (iii) far wings of the line shape remain quasistatic: $L(\omega) \rightarrow L_{qs}(\omega)$ for $|\omega| \gg \nu$. [In fact, (ii) can be considered a special case of (iii)].

Equation (18) can be rewritten as a function of the reduced detuning $\bar{\omega}$:

$$L(\bar{\nu}; \bar{\omega}) = \frac{1}{\pi} \operatorname{Re} \frac{J(\bar{\nu}; \bar{\omega})}{1 - \bar{\nu} J(\bar{\nu}; \bar{\omega})}, \quad (20)$$

where $\bar{\nu} = \nu/\Delta_0$ and

$$J(\bar{\nu}; \bar{\omega}) \equiv \int \frac{L_{qs}(\bar{\omega}')d\bar{\omega}'}{\bar{\nu} + i(\bar{\omega} - \bar{\omega}')}. \quad (21)$$

Rewriting Eq. (20) explicitly, one obtains

$$L(\bar{\nu}; \bar{\omega}) = \frac{1}{\pi} \frac{J^R - \bar{\nu} |J|^2}{1 - 2\bar{\nu} J^R + \bar{\nu}^2 |J|^2}, \quad (22)$$

where J^R is the real part of $J(\bar{\nu}; \bar{\omega})$ and its arguments were omitted for clarity.

The integral in Eq. (21) is a convolution of two functions, $L_{qs}(\bar{\omega})$ and $(\bar{\nu} + i\bar{\omega})^{-1}$. Using the convolution theorem, it can be represented as

$$J(\bar{\nu}; \bar{\omega}) = \mathcal{F}^{-1}\{\mathcal{F}\{L_{qs}(\bar{\omega})\}\mathcal{F}\{(\bar{\nu} + i\bar{\omega})^{-1}\}\}, \quad (23)$$

where \mathcal{F} and \mathcal{F}^{-1} designate the direct and inverse Fourier transforms, respectively. Noticing that for $\bar{\nu} > 0$

$$\mathcal{F}\{(\bar{\nu} + i\bar{\omega})^{-1}\}(\tau) = 2\pi e^{\bar{\nu}\tau} \theta(-\tau), \quad (24)$$

where $\theta(x)$ is the Heaviside step function [$\theta(x)$ is zero for negative x and unity for positive x], we obtain an alternative expression for $J(\bar{\nu}; \bar{\omega})$ which will be more convenient for our purposes:

$$J(\bar{\nu}; \bar{\omega}) = \int_0^\infty d\tau e^{-i(\bar{\omega}-i\bar{\nu})\tau} \mathcal{F}\{L_{qs}\}(-\tau). \quad (25)$$

We note that in the dipole approximation, $\mathcal{F}\{L_{qs}\}$ is formally identical to the autocorrelation function of the light amplitude [4], thus, one may write

$$J(\bar{\nu}; \bar{\omega}) = \int_0^\infty d\tau e^{-i(\bar{\omega}-i\bar{\nu})\tau} C_{qs}(\tau). \quad (26)$$

C. QC-FFM

We now substitute the general quasistatic line shape L_{qs} in Eq. (25) with the QC one (9). Therefore, using Eq. (11),

$$J(\bar{\nu}; \bar{\omega}) = \int_0^\infty d\tau \exp(-\tau^{3/2} - i(\bar{\omega} - i\bar{\nu})\tau) = T_{3/2}(\bar{\omega} - i\bar{\nu}), \quad (27)$$

where

$$T_\mu(z) \equiv \int_0^\infty d\xi \exp(-\xi^\mu - iz\xi). \quad (28)$$

Some properties of $T_\mu(z)$ are given in the Appendix.

Finally, Eq. (20) becomes

$$L(\bar{\nu}; \bar{\omega}) = \frac{1}{\pi} \operatorname{Re} \frac{T_{3/2}(\bar{\omega} - i\bar{\nu})}{1 - \bar{\nu} T_{3/2}(\bar{\omega} - i\bar{\nu})}. \quad (29)$$

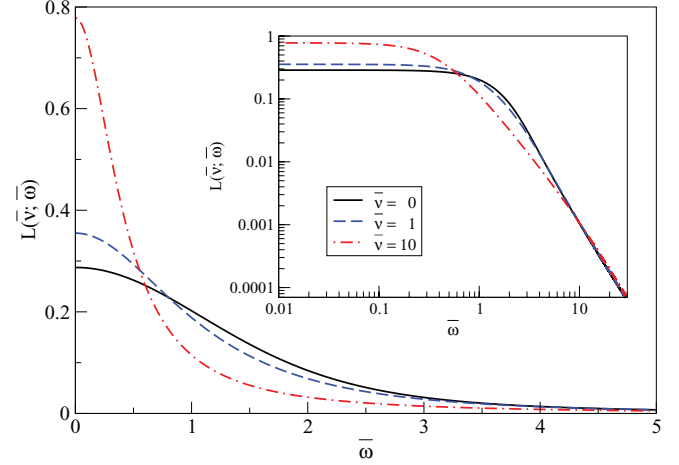


FIG. 2. (Color online) Line shapes as given by Eq. (29) for different values of $\bar{\nu}$.

Plots of $L(\bar{\nu}; \bar{\omega})$ for $\bar{\nu} = 0, 1$, and 10 are given in Fig. 2.

Evidently, $L(0; \bar{\omega})$ is exactly the quasistatic $S(\bar{\omega})$. For $\bar{\nu} = 1$, a deviation from the quasistatic profile is noticeable, and at $\bar{\nu} = 10$ the line becomes significantly narrower. Nevertheless, sufficiently far wings ($|\bar{\omega}| \gg \bar{\nu}$) remain quasistatic, clearly seen in the log-log scale shown in the inset of the figure.

III. DISCUSSION

A. Generalization to other broadening mechanisms

As shown in [2], the line shape given by Eq. (18) is functionally equivalent to the narrowing of the Doppler broadening (the Dicke effect [7]), obtained in the framework of the strong collisional model [8]. One is therefore tempted to generalize Eq. (29) to arbitrary μ 's:²

$$L_\mu(\bar{\nu}; \bar{\omega}) = \frac{1}{\pi} \operatorname{Re} \frac{T_\mu(\bar{\omega} - i\bar{\nu})}{1 - \bar{\nu} T_\mu(\bar{\omega} - i\bar{\nu})}. \quad (30)$$

Indeed, it can be straightforwardly shown, that, e.g., for $\mu = 2$, the above expression corresponds to the Doppler broadening. Evidently, the scaling constant Δ_0 used for switching from ω and ν to $\bar{\omega}$ and $\bar{\nu}$ would be different in this case: $\omega_0 v_{th}/\sqrt{2}c$ instead of $\alpha_{nn'} F_0/\hbar$ defined by Eq. (5).

B. Collision-dominated limit

Let us consider the line shape in the collision-dominated limit, i.e., for $\bar{\nu} \gg 1$. The central part of the profile ($|\bar{\omega}|/\bar{\nu} \ll 1$) can be obtained by substituting in Eq. (30) $T_\mu(\bar{\omega} - i\bar{\nu})$ with first two terms from its expansion series (A5):

$$L_\mu(\bar{\nu}; \bar{\omega}) \simeq \frac{1}{\pi} \frac{\frac{\Gamma(\mu+1)}{\bar{\nu}^{\mu-1}}}{\left[\frac{\Gamma(\mu+1)}{\bar{\nu}^{\mu-1}}\right]^2 + \bar{\omega}^2}, \quad (31)$$

²Actually, $0 < \mu \leq 2$; see Appendix.

i.e., a Lorentzian with HWHM $\bar{\gamma}_\mu = \frac{\Gamma(\mu+1)}{\bar{v}^{\mu-1}}$, or, in the usual units,

$$\gamma_\mu = \Gamma(\mu + 1)\Delta_0 \left(\frac{\Delta_0}{v}\right)^{\mu-1}. \quad (32)$$

For example, for the Doppler broadening ($\mu = 2$) this gives $\frac{2\Delta_0^2}{v}$, exactly as in [8]. Another interesting case to consider is the resonance broadening that has a Lorentzian ($\mu = 1$) line shape in the quasistatic approximation. According to Eq. (32), the shape in the impact limit remains Lorentzian with the same width $\gamma = \Delta_0$. Indeed, it is known that the collisional line width due to resonance broadening is independent of the velocity of perturbers [9].

We now return to the main subject of this study, i.e., the dynamic Stark line shapes in the QC-FFM approximation. In this case ($\mu = 3/2$),

$$\bar{\gamma}_{3/2} = \frac{\Gamma(5/2)}{\sqrt{\bar{v}}} = \frac{3\sqrt{\pi}}{4\sqrt{\bar{v}}} \quad (33)$$

and, therefore,

$$\gamma_{3/2} = \frac{3\sqrt{\pi}}{4}\Delta_0\sqrt{\frac{\Delta_0}{v}} \propto \frac{N_p^{5/6}}{T^{1/4}}. \quad (34)$$

This result is in evident contradiction to the expected N_p and, especially, T dependence of the impact limit of the Stark broadening (17). Below, we examine whether this is a real effect or a consequence of invalidity of an approximation (i.e., QC or FFM) used.

C. Comparison to computer simulations

Computer simulation (CS) methods occupy an important and unique place in plasma line broadening calculations [10]. Among other applications, results of CS calculations can be considered as those of *gedanken* experiments, allowing for “measurements” that are either unrealistic or even entirely impossible in real experiments. Indeed, the range of 2–3 orders of magnitude of \bar{v} that is needed to either validate or invalidate the T dependence of our approach (see Fig. 3) corresponds to 4–6 orders of magnitude in temperature, which is hardly possible in a real experiment, especially taking into account that the Stark broadening should be distinguished from contributions due to other broadening mechanisms, such as the Doppler one.

In this study we employ the CS method described in Ref. [11]. In the derivation, we assumed an ideal one-component plasma; therefore, in order to make the comparison justified, we used straight-line trajectories of unshielded (Coulomb) particles of a single species in the simulations. Specifically, we chose the H Ly δ ($n = 5$ to $n' = 1$) line, disabling interactions between levels with different n and fine-structure effects (again, these settings correspond to the assumptions used in Sec. II). $n = 5$ is high enough for the QC approximation to be used with a sufficient ($\sim 10\%$) accuracy, while being not too high for the CS calculations to become too resource intensive (recall that the computational time scales as $\propto (n^2 + n'^2)^3$ [11]).

Protons of density $N_p = 10^{14} \text{ cm}^{-3}$ were assumed for perturbers, with the temperature in the range of 0.1 eV to

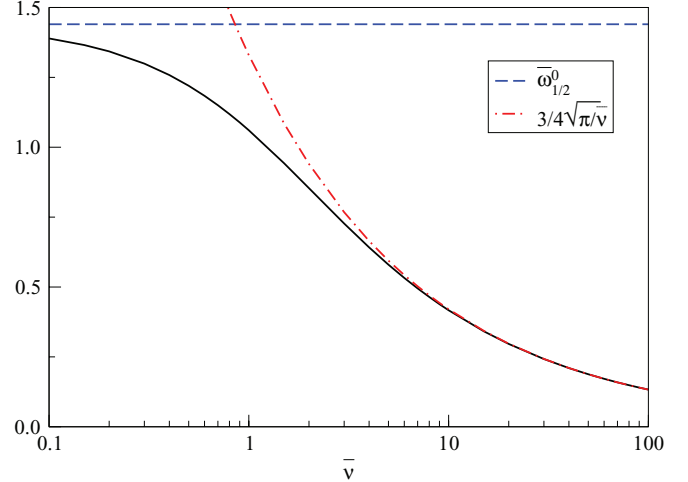


FIG. 3. (Color online) HWHM of $L(\bar{v}; \bar{w})$ as a function of \bar{v} (the solid line). $\bar{v} \rightarrow 0$ and $\bar{v} \rightarrow \infty$ asymptotes are shown by the dashed and dot-dashed lines, respectively.

100 keV, corresponding to $\bar{w}_{\text{dyn}} = w_{\text{dyn}}/\Delta_0$ from ≈ 0.14 to ≈ 140 ($\Delta_0 \approx 1.54 \times 10^{-4} \text{ eV}$, corresponding to $\approx 1.24 \text{ cm}^{-1}$ and $\approx 11.2 \text{ m\AA}$ in the wave-number and wavelength scales, respectively). 2000 particles were used in the simulations. The results are given in Fig. 4.

First, confirming previous findings [1], $R_0 = 0.5$ provides an optimal overall fit to the CS results. Second, both the original dynamical correction (16) and the FFM one (18) give nearly identical results up to $\bar{w}_{\text{dyn}} \lesssim 10$, provided that one chooses $C_0 = R_0$. However, in the collision-dominated regime, the two approaches disagree, as was discussed above (seen clearly in the log-log scale given in the inset of Fig. 4). In this region, the CS results show an unambiguous convergence

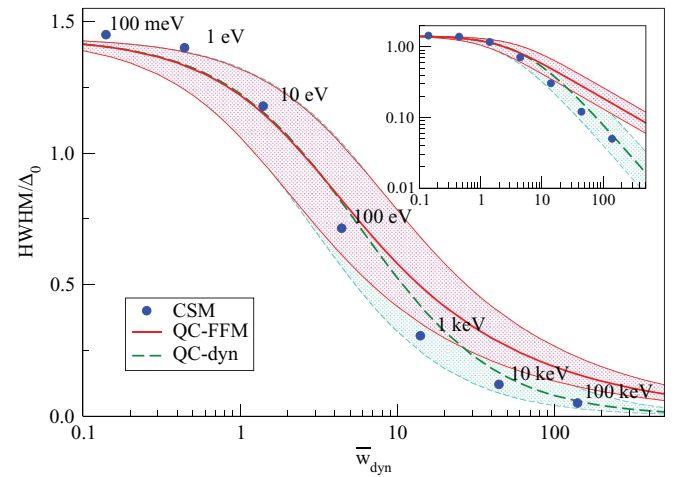


FIG. 4. (Color online) HWHM of the Stark broadening of H Ly δ due to proton perturbers with $N_p = 10^{14} \text{ cm}^{-3}$. Debye screening is neglected. CSM: computer simulation modeling results, annotated with the temperature assumed; QC-dyn: QC approximation with the original dynamical correction by Eq. (16); QC-FFM: line shapes calculated according to Eq. (29). The respective R_0 and C_0 empirical constants were assumed to be 0.5 and varied twofold in both directions, designated in the figure by hashed areas. The same data are shown in the inset graph in the log-log scale.

with the Eq. (16) variant, thus confirming the correct impact limit.

Thus, the FFM dynamic correction, while providing an excellent route to fast and accurate line-shape calculations up to moderate values of \bar{w}_{dyn} , fails in the $\bar{w}_{\text{dyn}} \gg 1$ region.³ It should be mentioned that, for practical purposes, the region of applicability is, as a rule, absolutely adequate for ion perturbers, however, for electrons it is not necessarily so. While it is possible (and, indeed, often done this way) to include the electron broadening via a convolution with a Lorentzian of an appropriate width (calculated in the impact approximation), a universal analytical approach is evidently desired.

D. Analysis and amendment

The reason that the universal expression for line shapes (30) describes the collision-affected Doppler broadening correctly, including the collision-dominated limit, but fails for the Stark broadening is, we believe, that the collision-induced fluctuation rate ν in Eq. (18) is assumed independent of the instantaneous value of the perturbation (directly related to the integration variable ω' in the same expression). Such an assumption is indeed justified for the Doppler broadening, where the rate of collisions with other particles depends rather weakly on the ‘‘perturbation’’ (the velocity of the emitter). However, in the case of the Stark broadening, both collisions and perturbation are due to the same mechanism (plasma micro-fields); thus, the assumption should be questioned.

Indeed, it can be shown that in an ideal plasma with the Holtmark microfield distribution (8), a ‘‘mean life’’ time t of a field F is the highest for fields around the most probable value and approaches zero in the $F \rightarrow 0$ and $F \rightarrow \infty$ limits as $t(F) \propto F$ and $t(F) \propto F^{-1/2}$, respectively [12]. Intuitively, $\bar{\nu} \sim 1/\tau$, therefore, fluctuation rates of very weak and very strong fields are higher than those of average fields.

One may, therefore, introduce a field-dependent frequency $\nu(\beta)$ instead of the constant one (19). It was shown [13] that such a modification indeed allows for attaining the proper impact limit. However, for a general $\nu(\beta)$ the line-shape calculations become analytically intractable. Instead, we attempt to semi-empirically construct an effective $\bar{\nu}(\bar{\nu})$, to be used instead of $\bar{\nu}$:

$$L(\bar{\nu}; \bar{\omega}) = \frac{1}{\pi} \text{Re} \frac{T_{3/2}(\bar{\omega} - i\bar{\nu})}{1 - \bar{\nu} T_{3/2}(\bar{\omega} - i\bar{\nu})}, \quad (35)$$

where $\bar{\nu}$ should satisfy the following requirements:

$$\bar{\nu} \rightarrow \begin{cases} \bar{\nu}, & \bar{\nu} \ll 1, \\ \propto \bar{\nu}^2, & \bar{\nu} \gg 1. \end{cases} \quad (36)$$

The $\bar{\nu} \propto \bar{\nu}^2$ asymptotic dependence ensures, according to Eq. (33), the correct impact limit. An obvious choice is

$$\bar{\nu} = \bar{\nu} + \frac{\bar{\nu}^2}{\bar{\nu}_0}, \quad (37)$$

where $\bar{\nu}_0$ can be inferred, e.g., by demanding that in the $\bar{\nu} \rightarrow \infty$ limit the line width asymptotically approaches

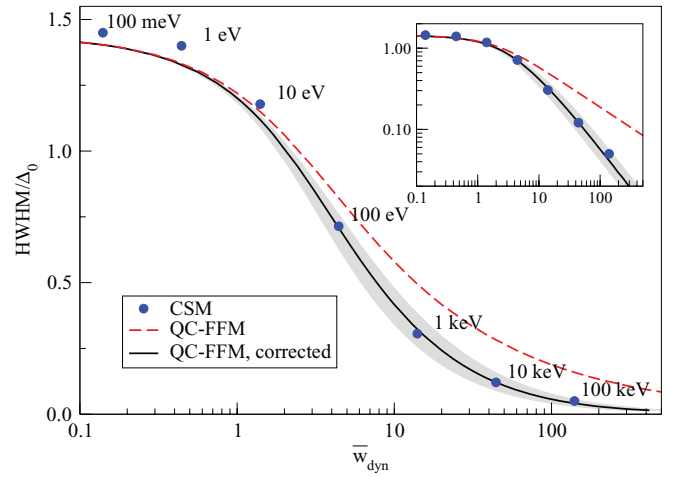


FIG. 5. (Color online) HWHM of the Stark broadening of H Ly δ under the same conditions as in Fig. 4. QC-FFM: line shapes calculated by Eq. (29); QC-FFM, corrected: line shapes calculated by Eqs. (35) and (37). The solid line corresponds to $\bar{\nu}_0 = 5$, while the hashed area around it indicates results obtained by varying $\bar{\nu}_0$ between 2.5 and 10.

Eq. (16), resulting in

$$\bar{\nu}_0^\infty = \frac{64(\bar{\omega}_{1/2}^0)^4}{9\pi} \approx 10. \quad (38)$$

By comparison with the CS results, it was determined that $\bar{\nu}_0 \approx 5$ gives the best overall fit, except for the highest (100 keV) temperature where $\bar{\nu}_0 \approx 8$ appears to be best. However, varying the parameter twofold in each direction shows a rather minor sensitivity to specific value. The results of the comparison are given in Fig. 5, where a very good agreement is seen over the whole range of temperatures considered. The significant improvement vs the noncorrected calculations is evident.

The line shapes, calculated using Eqs. (35) and (37) (with $\bar{\nu}_0 = 5$) are given in Fig. 6, together with respective

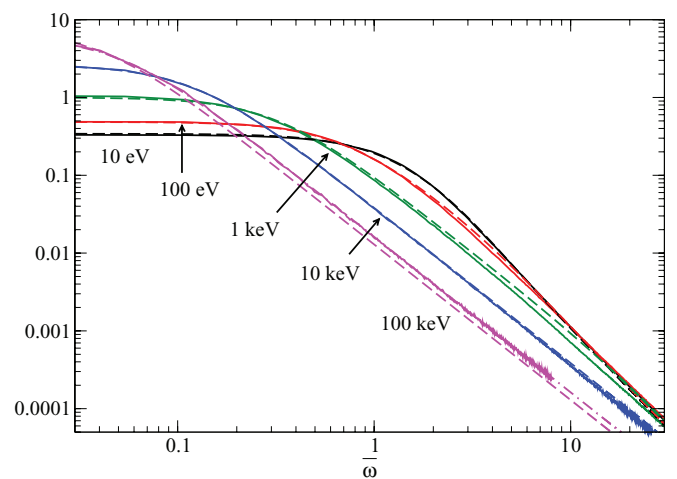


FIG. 6. (Color online) Line shapes of Stark-broadened H Ly δ under the same conditions as in Fig. 4. Solid lines: CS results. Dashed lines: analytical calculations with $\bar{\nu}_0 = 5$. Dot-dashed line: analytical calculation of the $T = 100$ keV case with $\bar{\nu}_0 = 8$.

³The failure to approach the impact limit was already noted in the first FFM paper [5].

CS-calculated profiles. Line shapes at $T = 0.1$ eV and 1 eV almost coincide with that at $T = 10$ eV, and therefore, are not shown for the sake of clarity.

It is seen that the universal analytical approach developed in the present study produces very good fits (typically within 10%) to the calculated line shapes over many orders of magnitude of temperature, with each one successfully describing entire profiles from the core of the line to very far (a few orders of magnitude of the respective HWHM) wings where the line intensity falls to several orders of magnitude relatively to its peak value. With the highest temperature assumed ($T = 100$ keV) the fit is less satisfactory (about 30% deviation). In this case, $\bar{\nu}_0 = 8$ produces an excellent fit, also shown in the figure. This may indicate that $\bar{\nu}_0^\infty \approx 10$ from Eq. (38) is indeed the correct limit and one should look for $\bar{\nu}$ in a more complex form than the simplest one assumed by Eq. (37). However, for practical purposes it suffices. Indeed, the field fluctuation rate due to protons at $T = 100$ keV corresponds to that due to electrons at $T_e \approx 100$ eV, significantly exceeding the temperature at which neutral H atoms would be fully ionized.

IV. REALISTIC PLASMAS

Up to now, we have assumed one-component ideal plasmas as the source of line broadening. In realistic calculations, these conditions are rarely met.

Accounting for more than one type of perturbers, in particular, for both ions and electrons, can be implemented by convolving line shapes imposed by each species separately, i.e.,

$$L_{\text{tot}}(\omega) = L_i(\bar{\nu}_i; \omega) * L_e(\bar{\nu}_e; \omega), \quad (39)$$

where “*” denotes convolution, and properly corrected (37) $\bar{\nu}_s$ for each species s is calculated using its charge, particle density, and temperature. Evidently, such an approach assumes that the effects of ions and electrons are independent. Although not rigorous, the approximation of independent electron and ion contributions to the line broadening proved to work very well in numerous calculations [4], due to the very different typical time scales of the respective (electronic and ionic) fields [14]. Our calculations, presented in the next section, also confirm the accuracy of this approximation. Note that in Eq. (39) we reverted from reduced $\bar{\omega}$ to ω , since Δ_0 (5) is, in general, different for each species. Generalization of Eq. (39) for plasmas composed of several ionic species is straightforward.

Correlation effects in plasma result in microfield distribution functions that deviate from the Holtsmark one (8). Although such distributions lack a simple analytical representation, fast and accurate methods for numerical evaluation of $W(\beta)$ are readily available [15]. Given that, it is possible to generalize the present approach for non-ideal plasmas. We first consider a situation when $W(\beta)$ is provided numerically, e.g., by the APEX method [16] or resulting from computer simulations. Let us return to Eq. (4) where no ideal-plasma assumption was made; its Fourier transform can be written as

$$\mathcal{F}\{L_{\text{qs}}(\bar{\omega})\}(\tau) \equiv C_{\text{qs}}(\tau) = -\text{Im} \tau^{-1} \mathcal{F}\{\beta^{-1} \bar{W}(\beta)\}(\tau). \quad (40)$$

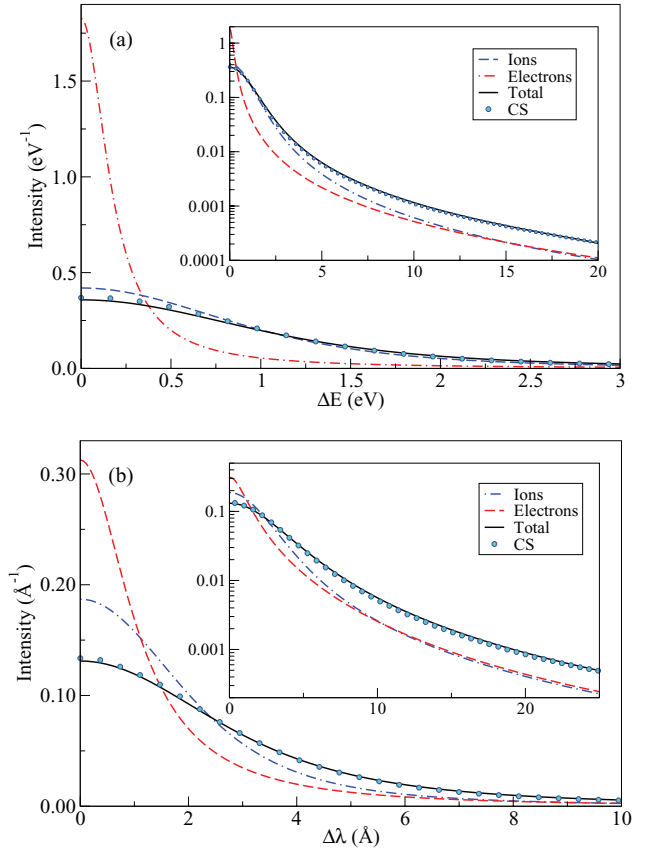


FIG. 7. (Color online) Comparison between analytical and computer simulation (CS) results of Stark broadening of (a) Ne X Ly δ in deuterium plasma with $N_e = 10^{21}$ cm $^{-3}$ and $kT = 1$ keV; (b) D Balmer $n = 9$ line in deuterium plasma with $N_e = 5 \times 10^{14}$ cm $^{-3}$ and $kT = 4$ eV.

Evidently, $W(\beta)$ and, hence, $C(\tau)$ depend parametrically on charges, densities, and temperatures of plasma species. Together with Eqs. (26) and (22), this gives the line-shape contribution due to a given species.

Equation (40) is suitable if $W(\beta)$ is given numerically. However, in many theoretical models (e.g., [17,18]) $W(\beta)$ is represented in a form analogous to that of the Holtsmark distribution (8), namely

$$W(\beta) = \frac{2}{\pi} \beta \int_0^\infty x \sin(\beta x) \exp[-f(x)] dx \quad (41)$$

[again, $f(x)$ depends on plasma parameters; for plasmas approaching ideality, $f(x) \rightarrow x^{3/2}$]. In such a case, a shorter route is available:

$$J(\bar{\nu}; \bar{\omega}) = \int_0^\infty d\tau \exp[-f(\tau) - i(\bar{\omega} - i\bar{\nu})\tau]. \quad (42)$$

In both cases, one should use $\bar{\nu}$ in place of $\bar{\nu}$ (37) in the right-hand side of Eq. (20) or (22).

V. EXAMPLES

As an example, given in Fig. 7(a) are calculation results for the shape of Lyman δ of H-like neon in a deuterium plasma with $N_e = 10^{21}$ cm $^{-3}$ and $kT = 1000$ eV (such a plasma may exist in mega-ampere deuterium-puff z -pinches, with neon

used as a dopant). The line shapes due to ions and electrons separately are shown by the dashed and dot-dashed curves, respectively, while the total line shape (solid line) is obtained by convolving these two shapes. For comparison, the line shape was also calculated using a computer simulation method [11]⁴ assuming the same plasma conditions, shown by the circle symbols. An excellent agreement over the entire line shape is evident, including the very far wings, where the line intensity falls by a few orders of magnitude relatively to its peak value; this is clearly seen in the log-log scale given in the inset of the figure. We also note that the asymptotic behavior of the far wings due to electrons is the same as that due to (singly charged) ions, as expected.

Another example is given in Fig. 7(b), where results of calculations for the deuterium $n = 9$ Balmer line for $N_e = 5 \times 10^{14} \text{ cm}^{-3}$ and $kT = 4 \text{ eV}$ (conditions typical for magnetic fusion experiments) are presented. Here again, an excellent agreement with the computer-simulation results is demonstrated over the entire line shape.

These examples demonstrate the applicability of the new method to a broad range of scientifically sound cases. The calculations are very fast, therefore it becomes practical to incorporate them into non-LTE plasma kinetics codes (e.g., [19–21]), compromising neither accuracy nor computational resources required. Furthermore, the computational time is independent of the principal quantum numbers of the transitions involved; therefore, the method can be easily applied to such complex phenomena as merging of the discrete and continuous spectra and ionization potential lowering due to plasma effects.

VI. APPLICABILITY

The present method is based on the QC approximation for the line shapes and, therefore, inherits the limitations of the parent method, discussed in the original study [1]. In particular, the QC approximation was derived assuming hydrogenlike transitions with $\Delta n \gg 1$. Nevertheless, it also describes rather well line shapes of transitions with Δn as low as 2. An example of such a transition is given in Fig. 8. Although the shape of the central region of the Balmer β line shape differs from that of the accurate calculations (evidently, the dip cannot be reproduced within the QC approximation), the widths agree within $\approx 10\%$, as do the intensities of the far line wings. We note, however, that for lines with $\Delta n = 1$, such as Lyman α or Balmer α , where the inaccuracy may be very significant, the method is inapplicable.

The validity of the dipole approximation is justified for electric fields that are weak enough for the higher-order-multipole corrections to remain small. Therefore, we require that the change of the plasma electric field is small on the spatial scale of the radiator size, i.e., for each perturber species p ,

$$\frac{n^2}{Z} a_0 N_p^{1/3} \ll 1. \quad (43)$$

⁴The agreement with other calculations and, where available, with experimental data was shown to be very good; see, e.g., [22].

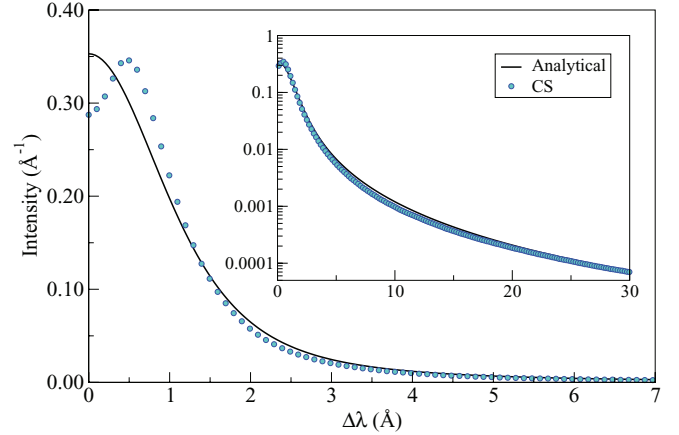


FIG. 8. (Color online) Comparison between analytical and computer simulation (CS) results of the Stark broadening of H Balmer β line in ideal deuterium plasma with $N_e = 10^{15} \text{ cm}^{-3}$ and $kT = 1 \text{ eV}$.

The neglect of the quenching interactions (i.e., those involving levels with different principal quantum numbers), resulting in deviations from the linear Stark effect, can be justified when the linear Stark effect of a given level is significantly smaller than the distance to the next neighboring level, i.e.,

$$\bar{\omega}_{1/2}^0 \alpha_n F_0 \ll \frac{Z^2 e^2}{2a_0} \left[\frac{1}{n^2} - \frac{1}{(n+1)^2} \right] \approx \frac{Z^2 e^2}{a_0 n^3}. \quad (44)$$

VII. CONCLUSIONS

By combining the QC approximation of the static Stark line shapes [1] and the FFM approach [2] for accounting for the dynamic effects, we derived an efficient and accurate method for calculating shapes of hydrogen and hydrogenlike transitions (including Rydberg ones) in plasmas. A semi-empiric amendment to FFM in the high-frequency domain was made, resulting in the correct impact-approximation limit and, thus, allowing for direct application of the method to both ion and electron perturbations alike. Comparisons with computer simulations showed excellent agreement.

ACKNOWLEDGMENTS

We gratefully acknowledge fruitful discussions with A. Calisti, A. Demura, H. R. Griem, J. D. Hey, and V. S. Lisitsa. Suggestions and comments by anonymous referees are highly appreciated. This work was supported in part by the Israel Science Foundation, the Minerva Foundation (Germany), and Sandia National Laboratories (USA).

APPENDIX: SOME PROPERTIES OF $T_\mu(z)$

Definition:

$$T_\mu(z) \equiv \int_0^\infty d\xi \exp(-\xi^\mu - iz\xi). \quad (A1)$$

The real part of T_μ of a real argument is, up to the factor of π , an unskewed, unshifted, and normalized stable distribution (defined for $0 < \mu \leq 2$; for $\mu \leq 0$ the integral diverges while

for $\mu > 2$ the function is not positive for arbitrary x):

$$\frac{1}{\pi} \operatorname{Re} T_{\mu}(x) = \frac{1}{2\pi} \int_{-\infty}^{\infty} d\xi \exp(-|\xi|^{\mu} - ix\xi). \quad (\text{A2})$$

In particular, $\mu = 1$ gives the Cauchy distribution (Lorentzian):

$$\frac{1}{\pi} \operatorname{Re} T_1(x) = \frac{1}{\pi} \frac{1}{1+x^2}, \quad (\text{A3})$$

while $\mu = 2$ corresponds to the normal distribution (Gaussian):

$$\frac{1}{\pi} \operatorname{Re} T_2(x) = \frac{1}{\sqrt{4\pi}} e^{-x^2/4}. \quad (\text{A4})$$

Evidently, $\mu = 3/2$ gives $S(x)$ from Eq. (10), which is called the Holtmark distribution in mathematical statistics and is often designated by $H(x)$, not to be confused with the

Holtmark field distribution (8) used in plasma physics and astronomy.

Expanding $\exp(-\xi^{\mu})$ in Eq. (A1) into a Taylor series, we obtain, provided $\operatorname{Im} z < 0$:

$$\begin{aligned} T_{\mu}(z) &= \int_0^{\infty} d\xi e^{-iz\xi} \sum_{n=0}^{\infty} \frac{(-\xi^{\mu})^n}{n!} \\ &= \sum_{n=0}^{\infty} \frac{(-1)^n}{n!} \int_0^{\infty} d\xi \xi^{\mu n} e^{-iz\xi} \\ &= \sum_{n=0}^{\infty} \frac{(-1)^n \Gamma(\mu n + 1)}{n!} \frac{1}{(iz)^{\mu n + 1}} \\ &= \frac{1}{iz} - \frac{\Gamma(\mu + 1)}{(iz)^{\mu + 1}} + \dots, \end{aligned} \quad (\text{A5})$$

where $\Gamma(z)$ is the gamma function.

-
- [1] E. Stambulchik and Y. Maron, *J. Phys. B: At. Mol. Opt. Phys.* **41**, 095703 (2008).
- [2] A. Calisti, C. Mossé, S. Ferri, B. Talin, F. Rosmej, L. A. Bureyeva, and V. S. Lisitsa, *Phys. Rev. E* **81**, 016406 (2010); L. A. Bureeva, M. B. Kadomtsev, M. G. Levashova, V. S. Lisitsa, A. Calisti, B. Talin, and F. Rosmej, *JETP Lett.* **90**, 647 (2010).
- [3] J. Holtmark, *Ann. Phys. (Leipzig)* **58**, 577 (1919).
- [4] H. R. Griem, *Spectral Line Broadening by Plasmas* (Academic, New York, 1974).
- [5] B. Talin, A. Calisti, L. Godbert, R. Stamm, R. W. Lee, and L. Klein, *Phys. Rev. A* **51**, 1918 (1995).
- [6] A. Calisti (private communication).
- [7] R. H. Dicke, *Phys. Rev.* **89**, 472 (1953).
- [8] S. G. Rautian and I. I. Sobel'man, *Sov. Phys. Usp.* **9**, 701 (1967).
- [9] H. R. Griem, *Principles of Plasma Spectroscopy* (Cambridge University Press, Cambridge, UK, 1997), Chap. 4.8, and references therein.
- [10] E. Stambulchik and Y. Maron, *High Energy Density Phys.* **6**, 9 (2010).
- [11] E. Stambulchik and Y. Maron, *J. Quant. Spectrosc. Radiat. Transfer* **99**, 730 (2006).
- [12] S. Chandrasekhar and J. von Neumann, *Astrophys. J.* **95**, 489 (1942).
- [13] V. S. Lisitsa (private communication).
- [14] S. Alexiou, *Phys. Rev. Lett.* **76**, 1836 (1996).
- [15] A. Demura, *Int. J. Spectrosc.* **2010**, 671073 (2010).
- [16] C. A. Iglesias, J. L. Lebowitz, and D. MacGowan, *Phys. Rev. A* **28**, 1667 (1983); C. Iglesias, F. Rogers, R. Shepherd, A. Bar-Shalom, M. Murillo, D. Kilcrease, A. Calisti, and R. Lee, *J. Quant. Spectrosc. Radiat. Transfer* **65**, 303 (2000).
- [17] M. Baranger and B. Mozer, *Phys. Rev.* **115**, 521 (1959); B. Mozer and M. Baranger, *ibid.* **118**, 626 (1960).
- [18] H. Pfennig and E. Treffitz, *Z. Naturforsch. A* **21**, 697 (1966).
- [19] Y. V. Ralchenko and Y. Maron, *J. Quant. Spectrosc. Radiat. Transfer* **71**, 609 (2001).
- [20] V. Fisher, D. Fisher, and Y. Maron, *High Energy Density Phys.* **3**, 283 (2007).
- [21] S. B. Hansen, *Can. J. Phys.* **89**, 633 (2011).
- [22] E. Stambulchik, S. Alexiou, H. R. Griem, and P. C. Kepple, *Phys. Rev. E* **75**, 016401 (2007).